

Rotational Spectroscopy and Conformational Flexibility of 2-Phenylethanethiol: The Dominant S–H... π Intramolecular Hydrogen Bond

Rizalina Tama Saragi,^[a, b] Wenqin Li,^[a] Marcos Juanes,^[a] Lourdes Enríquez,^[c] Ruth Pinacho,^[c] José Emiliano Rubio,^[c] and Alberto Lesarri^{*[a]}

This article is dedicated to Professor Martín Jaraíz on occasion of his 70th birthday, for his inspiration in science.

We present a rotational-computational investigation of the aromatic mercaptan 2-phenylethanethiol, addressing its potential energy surface, conformational equilibrium, internal dynamics and intramolecular interactions. The experiment used broadband chirped-pulse Fourier transform microwave spectroscopy in a supersonic jet expansion, recording the rotational spectrum in the 2–8 GHz frequency region. Two different conformers were detected in the spectrum. The most intense transitions correspond to a skew (*gauche-gauche*) conformation, identified as the global minimum. The spectra of ten different isotopologues were assigned for this species, leading to accurate

effective and substitution structures. The weaker spectrum presents small tunnelling doublings caused by the torsional motion of the thiol group, which are only compatible with an *antiperiplanar* skeleton and a *gauche* thiol. The larger stability of the global minimum is attributed to an intramolecular S–H... π weak hydrogen bond. A comparison of the intramolecular interactions in the title molecule and 2-phenylethanol, similarly stabilized by a O–H... π hydrogen bond, shows the different strength of these interactions. Density functional (B3LYP-D3, B2PLYP-D3) and *ab initio* (MP2) calculations were conducted for the molecule.

1. Introduction

2-Phenylethanethiol (phenethyl mercaptan, later PET) is an aromatic compound with a flexible 2-carbon side chain connecting the phenyl ring and the thiol group (Ph–(CH₂)₂–R, R=SH). Thiols have typically pungent odors and are not common mammal metabolites. However, they are used biologically as defensive weapons by musteloids and as chemical signaling molecules by canids.^[1] In particular, the phenylethane group is generated in secretory glands of the anal sacs of skunks (species *Mephitis macroura* and *Mephitis mephitis*) to produce their foul-smelling defensive spray.^[2,3] The title compound can also be used as flavoring agent or adjuvant.^[4]

Technological applications of alkylthiols include the construction of photo-functional self-assembled monolayers,^[5,6] which exploit the chemisorption of sulfur to metals. From a structural point of view PET may orient its polar thiol group around the ring, plausibly giving rise to several competing conformations. In 2-phenylethanol the skew global minimum (Gg π) benefits from a O–H... π intramolecular hydrogen bond to the ring, but five other conformations are also available below 8 kJ mol⁻¹. The structural preferences of the alcohol have been confirmed using mass-resolved resonance-enhanced multiphoton ionization (R2PI),^[7] double-resonance IR/UV ion-dip,^[8–10] ionization-loss stimulated Raman^[11] and microwave spectroscopy,^[12,13] which detected the global minimum and a second plane-symmetric isomer (At). Since the larger size and polarizability of sulfur is expected to decrease or modulate the hydrogen bonding capabilities of PET,^[14,15] it is interesting to check which changes are introduced in the conformational landscape by the replacement of the oxygen atom by sulfur and whether a S–H... π weak hydrogen bond prevails in the bare molecule. A previous electronic analysis of PET using R2PI^[16] detected two different species, but suggested that the second conformer differs from the alcohol in the orientation of the thiol group. However, no high-resolution study of PET is available, preventing the structural determination and observation of intramolecular dynamical effects associated to the thiol torsion.^[17–19] Here we present a multi-isotopic rotationally resolved analysis of PET, leading to an unambiguous discrimination of its conformational landscape and structure. This investigation complements previous rotational studies on other aromatic chalcogens like thiophenol,^[18–20] benzyl mercaptan,^[21,22] or selenophenol^[23] and

[a] Dr. R. Tama Saragi, W. Li, Dr. M. Juanes, Prof. Dr. A. Lesarri
Departamento de Química Física y Química Inorgánica – I.U. CINQUIMA,
Facultad de Ciencias, Universidad de Valladolid, Paseo de Belén 7, 47011
Valladolid, Spain
E-mail: alberto.lesarri@uva.es

[b] Dr. R. Tama Saragi
Present address: Institut für Ionenphysik und Angewandte Chemie, Uni-
versität Innsbruck, Technikerstr. 25/4. OG, 6020 Innsbruck, Austria

[c] Prof. Dr. L. Enríquez, Prof. Dr. R. Pinacho, Prof. Dr. J. E. Rubio
Departamento de Electrónica, ETSIT, Universidad de Valladolid, Paseo de
Belén 11, 47011 Valladolid, Spain

Supporting information for this article is available on the WWW under
<https://doi.org/10.1002/cphc.202300799>

© 2024 The Authors. ChemPhysChem published by Wiley-VCH GmbH. This is an open access article under the terms of the Creative Commons Attribution Non-Commercial NoDerivs License, which permits use and distribution in any medium, provided the original work is properly cited, the use is non-commercial and no modifications or adaptations are made.

will permit future studies of intermolecular complexes involving PET.

2. Results and Discussion

2.1. Potential energy surface

Similarly to 2-phenylethanol,^[7–13] the potential energy surface of PET is described with three torsion dihedrals associated to the terminal side chain. Density functional and *ab initio* calculations predicted five stable structures within 8 kJ mol⁻¹, shown in Figure 1. The predicted rotational, centrifugal and energetic parameters are collected in Tables S1–S3. For comparison, new B2PLYP calculations for 2-phenylethanol are shown in Table S4. All PET conformers share a near-perpendicular arrangement of C_β, as in the ethylbenzene prototype,^[24] benzyl alcohol^[25] or benzyl mercaptan.^[21] However, the predicted conformers differ in the orientation of the thiol group (dihedrals $\tau_1 = \text{SC}_\beta\text{--C}_\alpha\text{C}_{\text{ipso}}$ and $\tau_2 = \text{HS--C}_\beta\text{C}_\alpha$). The most stable Gg π conformer maintains *gauche-gauche* thiol orientations ($\tau_1 = \mp 66^\circ$, $\tau_2 = \pm 61^\circ$), permitting an intramolecular hydrogen bond to the phenyl ring. The second conformer Ag is predicted with an *antiperiplanar* sulfur skeleton and a *gauche* terminal hydrogen ($\tau_1 = \mp 177^\circ$, $\tau_2 = \mp 63^\circ$), while the fourth and fifth conformers Gg and Gt are also based on a *gauche* sulfur atom but adopt alternative staggered orientations of the thiol hydrogen atom. The third conformer At is the only plane-symmetric (C_s) structure. All non-symmetric conformers display two transient enantiomeric species. The atomic coordinates for the five most stable PET conformers are collected in Tables S5–S9.

2.2. Rotational Spectrum

The rotational spectrum of Figure 2 unequivocally resolved the structural properties of PET. Two different sets of rotational transitions were assigned in the experiment, confirming the presence of two conformers in the gas phase. The most intense spectrum was dominated by strong Q ($J \leftarrow J$) and R-branch ($J + 1 \leftarrow J$) μ_b transitions, accompanied by a set of R-branch μ_a transitions. The measured frequencies, covering quantum numbers below $J = 13$ and $K_{-1} = 4$, are collected in Table S10. The spectrum was reproduced to experimental accuracy with a semirigid rotor Watson's Hamiltonian including quartic centrifugal distortion terms,^[26] as implemented in Pickett's CALPGM programs.^[27] The fit results for this conformer are shown in Table 1. The intensity of the PET spectrum additionally permitted the observation of all nine ¹³C and ³⁴S monosubstituted isotopologues in natural abundance (ca. 1% and 4%, respectively), which were fitted similarly, fixing the centrifugal distortion terms to the parent isotopologue. The derived rotational parameters for the monoisotopic species are presented in Table 2, while the measured transition frequencies are collected in Tables S11–S19. The isotopic information permitted the determination of the PET structure without recourse to theoretical predictions, confirming the detection of isomer Gg π . Nevertheless, the computational predictions also support the observation of the global minimum, whose non-symmetric (C₁) structure impedes a double-minimum thiol inversion and the presence of tunnelling effects in the spectrum, as observed.

Following the identification of conformer Gg π , a second weaker spectrum, composed exclusively of R-branch μ_a transitions ($J < 7$ and $K_{-1} < 4$), was assigned separately. The second

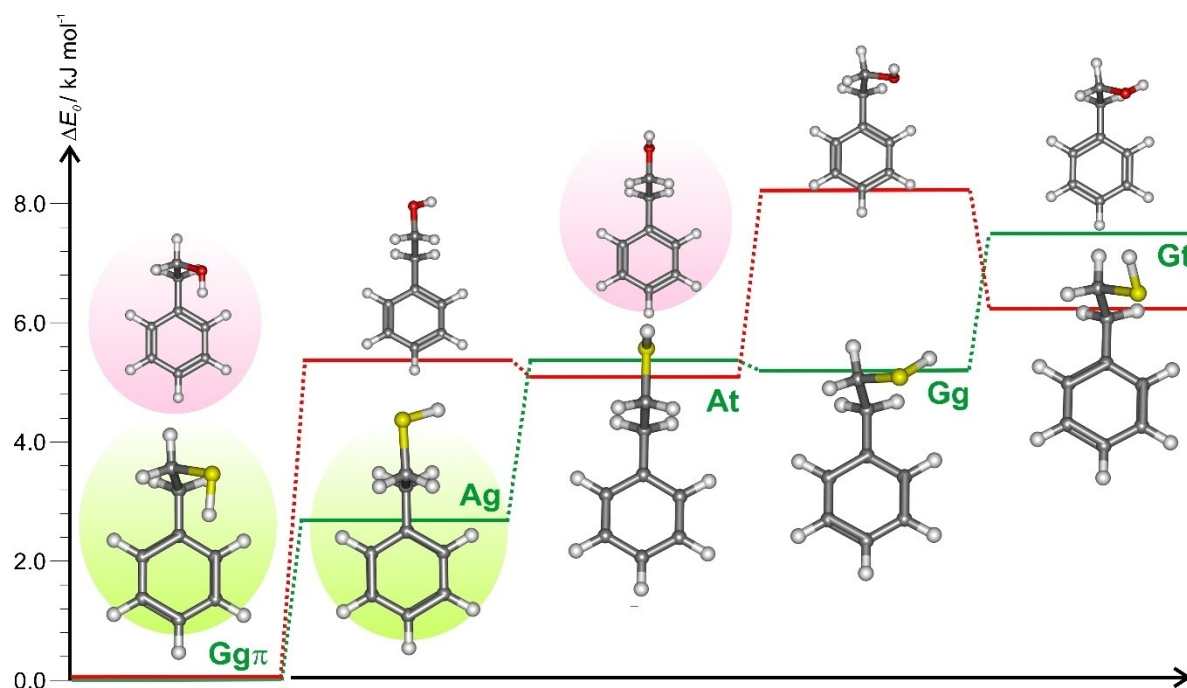


Figure 1. The five most stable conformers of 2-phenylethanethiol and 2-phenylethanol, showing the different conformational ordering and their relative energy values (B2PLYP-D3(BJ)/def2-TZVP, ZPE corrected, kJ mol⁻¹). See Tables S1–S3 for alternative B3LYP and MP2 calculations. The observed conformers of the two molecules are encircled. Conventional yellow and red coloring is used for sulfur and oxygen, respectively.

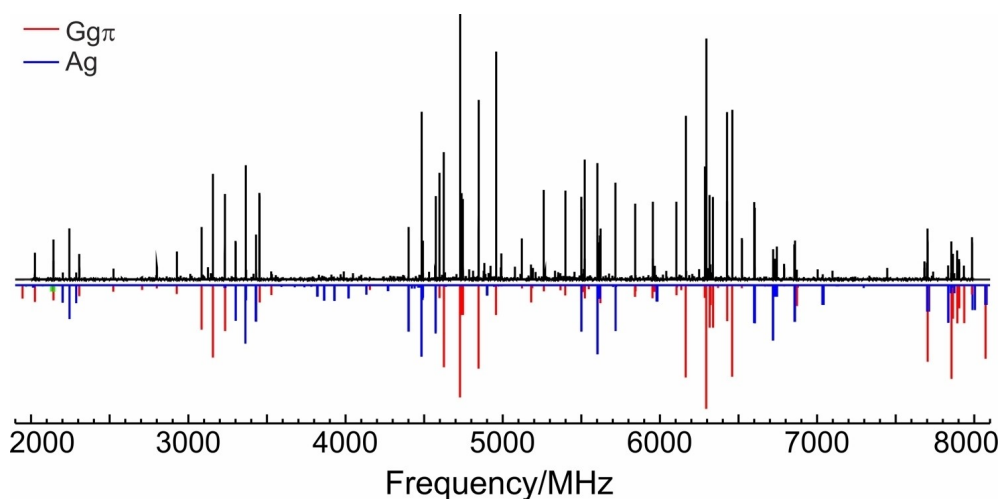


Figure 2. Rotational spectrum of 2-phenylethanethiol in the 2–8 GHz frequency region. The positive trace shows the experimental spectrum; the negative trace is the simulation of fitted rotational constants for the two isomers of the monomer. Small splittings in conformer Ag are not shown in this scale.

Table 1. Rotational parameters of the two observed conformers of 2-phenylethanethiol (parent species). The experiment corresponds to the ground-state observations, while theory represents equilibrium values.

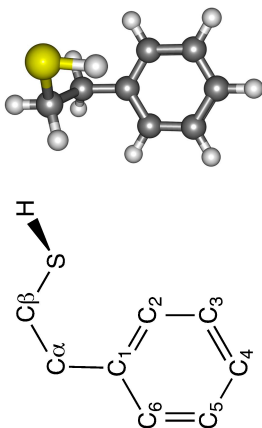
	Conformer Ggπ		Conformer Ag		Theory
	Experiment	Theory	Experiment $\nu=0$	$\nu=1$	
A (MHz) ^[a]	2700.35422(56) ^[c]	2712.18	4337.5(30)		4389.13
B (MHz)	826.62097(11)	830.81	582.8030(23)	582.7305(48)	582.04
C (MHz)	752.72166(12)	750.36	539.3944(24)	539.4658(48)	539.27
D_J (kHz)	0.2056(11)	0.169	0.028(17)		0.022
D_{JK} (kHz)	−0.0340(70)	2.194	1.118(66)		1.158
D_K (kHz)	1.560(88)	−0.912	[0.639] ^[d]		0.639
d_1 (Hz)	3.60(18)	−0.024	[−0.002]		−0.002
d_2 (Hz)	−9.760(72)	0.018	[0.002]		0.002
$ \mu_a $ (D)	+++	1.0	++		1.4
$ \mu_b $ (D)	+++	1.2	−		0.6
$ \mu_c $ (D)	++	0.2	−		0.1
N ^[b]	93		84		
σ (kHz)	3.8		25.8		

[a] Rotational constants (A , B , C), Watson's S -reduction centrifugal distortion constants (D_J , D_{JK} , D_K , d_1 , d_2) and electric dipole moments (μ_α , $\alpha=a$, b , c). [b] Number of transitions (N) and rms deviation (σ) of the fit. [c] Standard errors in parentheses in units of the last digit. [d] Values of the centrifugal distortion in square brackets were fixed to the ab initio values of Table S1 (B3LYP-D3(BJ)/def2-TZVP).

spectrum is characterized by the presence in some transitions of small (< 1 MHz) tunnelling doublings, illustrated in Figure 3. The tunnelling effects indicate the presence of an intramolecular large-amplitude motion, splitting the ground vibrational state in two torsional sublevels with independent rotational stacks. The initial inspection of the rotational constants confirmed the detection of the second predicted conformer Ag, with thiol inverting between the two sides of the plane-symmetric (C_s) all-*antiperiplanar* organosulfur sidechain. Similarly to benzyl mercaptan,^[21] the non-inverting intra-state ($\nu=0\leftarrow 0$ or $1\leftarrow 1$) μ_a rotational transitions show the smaller splittings, but give no information on the torsional energy

difference, so they could be fitted independently for each torsional sublevel. Conversely, the tunnelling-dependent splittings in the μ_b inverting transitions ($\nu=1\leftarrow 0$ or $0\leftarrow 1$) were not observed. Considering that the torsional difference could be similar to the value in benzyl mercaptan ($\Delta E_{01} = 2180.7$ MHz),^[21] we estimate that the splittings in the μ_b transitions would span several GHz, so their observation would require a much larger spectral bandwidth. Because of the small number of split transitions for conformer Ag only the B and C rotational constants were determined independently, floating two centrifugal distortion constants and freezing others to the predicted

Table 2. Ground-state rotational parameters of the isotopologues of 2-phenylethanethiol Ggπ, including all ¹³C and ³⁴S monosubstituted species in natural abundance.



Isomer Ggπ ³⁴ S	¹³ C(β)	¹³ C(α)	¹³ C(1)	¹³ C(2)	¹³ C(3)	¹³ C(4)	¹³ C(5)	¹³ C(6)
A (MHz) ^(a)	2677.32712(68) ^(d)	2688.33894(96)	2692.9782(14)	2677.1038(14)	2682.5749(15)	2693.65565(95)	2674.5784(16)	2679.40128(86)
B (MHz)	809.37357(20)	823.99094(24)	826.09110(55)	824.73059(51)	818.31510(60)	815.86285(34)	820.78424(58)	824.59286(35)
C (MHz)	737.68653(21)	747.14190(34)	752.36870(55)	749.58642(51)	45.97761(56)	743.73290(33)	746.24150(53)	751.24101(31)
N ^(b)	47	31	28	31	25	30	30	29
σ (kHz)	6.7	8.5	10.5	12.5	11.7	8.3	13.6	6.4

[a] Rotational constants (A, B, C). The Watson's S-reduction centrifugal distortion constants were fixed to the values: $D_1 = 0.206$ kHz, $D_{JK} = -0.034$ kHz, $D_K = 1.565$ kHz, $d_1 = 0.0036$ kHz, $d_2 = -0.0098$ kHz. [b] Number of transitions (N) and rms deviation (σ) of the fit. [c] Standard errors in units of the last digit.

values of Table S1. The results of the fit are shown in Table 1. The observed transition frequencies are listed in Table S20.

No additional species from the PET monomer were observed in the spectrum. We examined computationally some potential barriers for conformer interconversion using B3LYP-D3(BJ). Potential barriers around the sulfur dihedral ($SC_\alpha C_\beta C_{ipso}$), like those converting Ag to Ggπ or Gg to Ag in Figure S1 exceed 11 kJ mol⁻¹. This value is consistent with the experimental observation of the two most stable isomers, as empirical evidence suggests that for a single torsional degree of freedom barrier thresholds above ca. 5 kJ mol⁻¹ would impede conformational relaxation in the supersonic jet.^[28,29] At the same time, the three higher-energy conformers are expected to be simply depopulated at the conformational temperatures of 135 – 150 K previously estimated for similar jet experiments.^[30,31] Conversely, the thiol barriers around $HSC_\beta C_\alpha$ are much smaller, with the DFT calculations in Figure S2 suggesting a barrier of 3.4 kJ mol⁻¹ for the At to Ag conversion. This value represents a ca. 25% reduction compared with the calculated barrier of 4.5 kJ mol⁻¹ for 2-phenylethanol (MP2/6-31G(d,p)).^[12]

2.3. Molecular structure

Effective (r_o) and substitution (r_s) structures were calculated for conformer Ggπ of PET. Both methods have been described elsewhere.^[32] The effective method provided a description of the ground-state structure using a least-squares fit of structural parameters to the 30 experimental moments of inertia. Fits of different structural sets were tested using Rudolph's ru212 program,^[33,34] assuming a planar benzene ring and fixing the positions of the hydrogen atoms to the B3LYP-D3(BJ) structure. In the fit of Tables 3 and S21–S22 the (C–S) and all eight (C–C) independent interatomic distances were floated, together with two bond angles ($S-C_\beta-C_\alpha$, $C_\beta-C_\alpha-C_{ipso}$) and the ($S-C_\beta-C_\alpha-C_{ipso}$) dihedral of the side chain. This fit reproduces all the experimental rotational constants below 0.3 MHz with a satisfactorily global rms residual of 0.13 MHz (rms correlation coefficient of 0.39). More advanced calculations, in particular Watson's mass-dependent r_m method,^[35] were not successful. This is attributed to the need of three to six additional isotopic-dependent parameters, which would require additional isotopic data.^[23] Alternatively, the substitution method approximates the equilibrium coordinates using the Kraitchman equations,^[36] based on differences between isotopic moments of inertia. The calculated (unsigned) substitution coordinates are shown in Table S23. The uncertainties associated to this method were estimated using the empirical Costain errors, inversely proportional to the coordinate magnitude ($\delta z = K/|z|$).^[37] However, this method is known to produce unreliable results for small atomic coordinates,^[32,33,38] as is the case here for atom C_β . As a consequence, some substitution structural parameters are ill-determined, as illustrated by the small (C_β –S) distance and the larger differences between the calculated bond distances and the equilibrium structure compared to the effective structure. The structural information obtained from the isotopic data is compared with the computational predictions in Table 3.

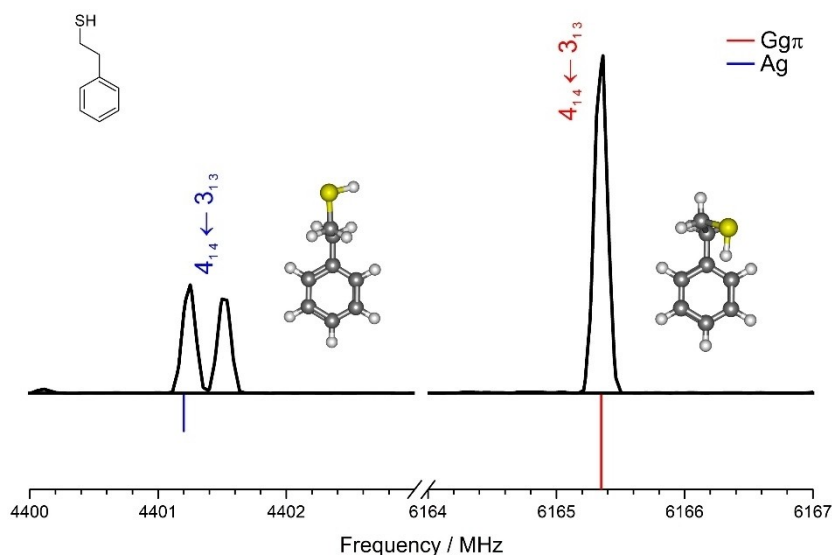


Figure 3. A typical rotational transition ($4_{1,4} \leftarrow 3_{1,3}$) of 2-phenylethanethiol, illustrating the tunnelling splittings in the μ_a -transitions of conformer Ag (left). Transitions from conformer Gg π (right) are not split.

Table 3. Molecular structure of 2-phenylethanethiol Gg π , and comparison with the theoretical predictions (B3LYP-D3(BJ)/def2-TZVP).

	r_0 ^[a]	r_s ^[b]	Theory ^[c]
$r(\text{S-H})$ (Å)	[1.3433] ^[d]		1.3433
$r(\text{C}_\beta\text{-S})$ (Å)	1.824(8) ^[e]	1.785(4) ^[f]	1.8262
$r(\text{C}_\alpha\text{-C}_\beta)$ (Å)	1.470(16)	1.611(9)	1.5328
$r(\text{C}_{\text{ipso}}\text{-C}_\alpha)$ (Å)	1.495(18)	1.447(5)	1.5055
$r(\text{C}_2\text{-C}_{\text{ipso}})$ (Å)	1.412(10)	1.430(5)	1.3940
$r(\text{C}_3\text{-C}_2)$ (Å)	1.403(18)	1.402(2)	1.3905
$r(\text{C}_4\text{-C}_3)$ (Å)	1.390(11)	1.392(4)	1.3890
$r(\text{C}_5\text{-C}_4)$ (Å)	1.404(12)	1.391(4)	1.3908
$r(\text{C}_6\text{-C}_5)$ (Å)	1.387(19)	1.409(3)	1.3884
$\angle(\text{C}_\alpha\text{-C}_\beta\text{-S})$ (deg)	118.2(7)	112.3(3)	114.68
$\angle(\text{C}_{\text{ipso}}\text{-C}_\alpha\text{-C}_\beta)$ (deg)	114.1(7)	109.3(3)	113.01
$\tau(\text{C}_\alpha\text{-C}_\beta\text{-S-H})$ (deg)	[61.19]		61.19
$\tau(\text{C}_{\text{ipso}}\text{-C}_\alpha\text{-C}_\beta\text{-S})$ (deg)	62.6(7)	69.3(5)	65.85

[a] Effective structure [b] Substitution structure [c] B3LYP-D3(BJ)/def2TZVP calculation [d] Values in square brackets were fixed to the computational prediction. [e] Standard deviation in units of the last digit for the r_0 fit. The estimated errors do not include possible uncertainties associated to the fitting model. [f] Uncertainties of the r_s substitution structure according to the Costain estimates.

2.4. Intramolecular hydrogen bonding

The most relevant chemical question in PET is the prevalence of an intramolecular interaction in the global minimum of PET, despite the weaker character of the S-H $\cdots\pi$ hydrogen bond compared to the O-H $\cdots\pi$ interaction in 2-phenylethanol. Non-covalent interactions were compared quantitatively in both molecules using Johnson-Contreras dimensionless reduced electronic density gradient ($s = \frac{1}{2(3\pi^2)^{1/3}} \frac{|\nabla\rho|}{\rho^{4/3}}$)^[39] In this method

isosurfaces of the reduced gradient in regions of low electronic density can be used to map non-covalent interactions. A distinction between attractive and repulsive interactions comes from the sign of one of the eigenvalues (λ_2) of the electronic density Hessian. Spatial maps of the reduced electronic density gradient for PET and 2-phenylethanol are shown in Figure 4, revealing broad regions of weak interaction above the ring associated to the hydrogen bond between the polar groups and the π clouds. The representation of the reduced electronic density gradient versus the signed electronic density shows in both molecules a minimum at negative abscissa, associated to the S-H $\cdots\pi$ and O-H $\cdots\pi$ interactions. Characteristically of this representation, the minima corresponding to PET appears at less negative values (> -0.01), confirming not only the presence of the S-H $\cdots\pi$ weak hydrogen bond, but also its smaller strength compared to O-H $\cdots\pi$, as expected from the lower electronegativity of sulfur.

3. Conclusions

A rotational-computational investigation of 2-phenylethanethiol has revealed the main features of its potential energy surface, conformational equilibrium, structural properties, and intramolecular non-covalent interactions. The experiment used broadband high-resolution rotational spectroscopy, leading to the identification of two different species in the gas phase, positively identified with the molecular global minimum and the second most stable species. The good intensity and high dynamical range of the experiment further permitted the assignment of the independent rotational spectra of nine additional isotopologues of the global minimum, corresponding to all monosubstituted ^{13}C -carbon and ^{34}S -sulfur species in natural abundance. In all cases the spectrum is reproduced with a semirigid rotor model with no tunnelling effects. Moreover,

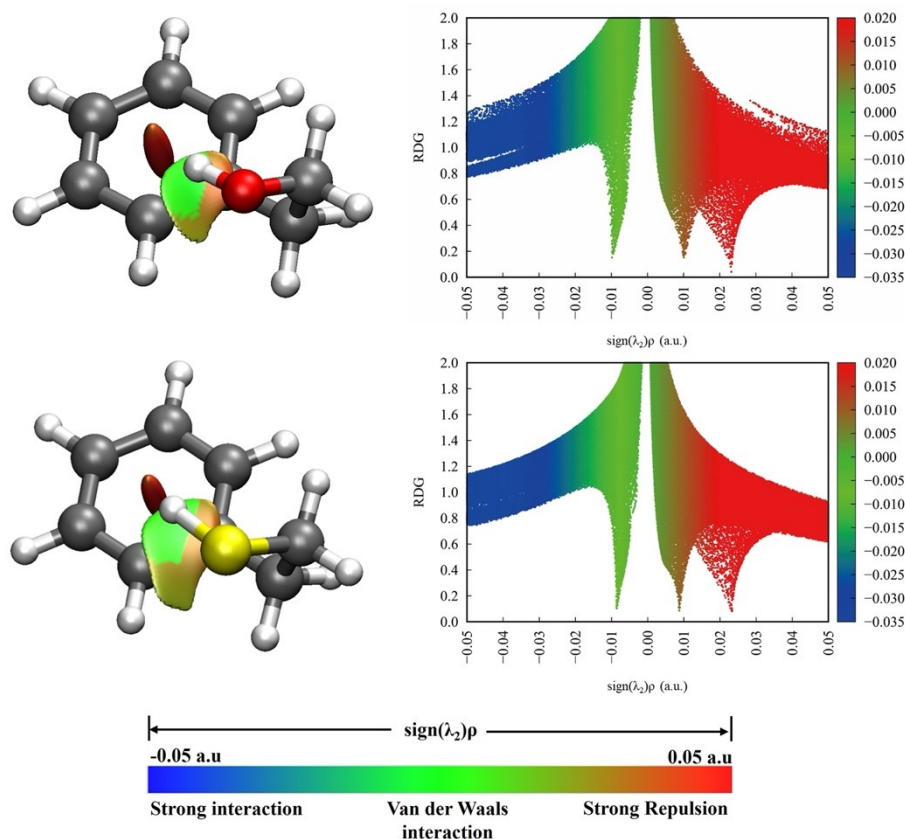


Figure 4. Non-covalent interaction plot for the global minimum of 2-phenylethanethiol (lower panel) and 2-phenylethanol (upper panel), together with the representation of the reduced electronic density gradient versus the signed electronic density for both molecules.

the availability of isotopic satellites for all the heavy atoms resulted in the experimental determination of effective and substitution structures for the molecular skeleton. The spectral and computational evidence indicates that molecular stabilization in the global minimum is the result of intramolecular forces associated to a weak S–H... π hydrogen bond, linking the polar group to the π cloud and resulting in a skew unsymmetric structure. In consequence, intramolecular hydrogen bonding is confirmed as dominant structural factor not only in 2-phenylethanol, but also in the thiol. The analysis of the reduced gradient of the electronic density confirms the weaker attractive character of the thiol interaction. Other S–H... π interactions, often in combination with S–H...S hydrogen bonds, have been found on gas-phase thiol dimers,^[22,40,41] but the experimental information is still small compared to alcohols.^[14,15]

Unlike the global minimum, the rotational spectrum of the second conformer shows small tunnelling splittings, confirming a large-amplitude double-minimum torsional motion consistent with a symmetric *antiperiplanar* carbon skeleton and two *gauche* \pm orientations of the thiol group. The presence of tunnelling effects is the most compelling proof of the intramolecular dynamics, which otherwise could not be assessed using only vibrational information. The second conformer thus differs from the alcohol, where both the terminal group and the carbon skeleton adopt an *antiperiplanar* C_s -symmetric structure. This difference is associated to the smaller torsional barriers on

descending the chalcogen group, as illustrated in the cases of phenol ($B_2^{exp} = 1207 \text{ cm}^{-1}$),^[18] thiophenol ($B_2^{exp} = 289 \text{ cm}^{-1}$)^[19] and selenophenol ($B_2^{theory} = 42 \text{ cm}^{-1}$).^[23] The three higher-energy conformers were not observed experimentally, either because of conformational relaxation (in case of thiol torsion paths) or depopulation.

In summary, the present work offers high-resolution spectroscopic and computational data for 2-phenylethanethiol, complementing the available vibrational information and expanding our understanding of the conformational properties of aromatic thiols and the nature of sulfur-centered hydrogen bonds, less studied in the gas-phase but often reported in biomolecular crystallographic studies. This investigation shows also the structural differences with the related alcohol and will permit future work on intermolecular clusters of PET, in particular the homodimer and the hydrates.

Experimental and Computational Methods

The sample of 2-phenylethane thiol (>97%, b.p. 491 K) was obtained commercially and received no further purification. The compound was vaporized inside the heating reservoir of a pulsed solenoid-driven gas injector at mild temperatures (318–328 K). The sample vapors were co-expanded near adiabatically with an inert carrier gas, using a circular nozzle (0.8 mm diameter). Neon at stagnation pressures of 0.2 MPa was used as carrier gas, with typical

molecular pulses of 800–900 μ s. The expanding supersonic jet was probed in the 2–8 GHz cm-wave region with a direct-digital chirped-pulse Fourier transform microwave (CP-FTMW) spectrometer.^[42] The spectrometer operating sequence was based in series of short (4 μ s, 20 W) chirped pulses, which were broadcasted perpendicularly to the jet. The MW radiation produces a linear fast-passage broadband transient excitation.^[43,44] Simultaneously covering the full spectral bandwidth. Following the microwave excitation, the molecular ensemble emits a free-induction decay, which is detected in the time-domain (ca. 40 μ s) and digitally recorded using a 20 MSamples/s oscilloscope. A Fourier transformation with a Kaiser-Bessel window results in FWHM linewidths smaller than 150 kHz. In this experiment ca. 1 M averages were acquired at a repetition rate of 5 Hz. The uncertainty of the frequency measurements was estimated below 20 kHz.

Several computational calculations complemented the experiments. Following an initial conformational screening with molecular mechanics (MMFFs^[45]), all further calculations used density-functional theory (DFT) or second-order Møller-Plesset ab initio perturbation method.^[46] Two density-functionals were selected here, including the hybrid B3LYP^[47] and the double hybrid B2PLYP^[48] methods. DFT calculations were supplemented with D3^[49] dispersion corrections and Becke-Johnson damping.^[50] The Ahlrichs' polarized triple- ζ basis def2-TZVP^[51] was used in all cases. Vibrational frequency calculations were performed at the same level of theory, using the harmonic approximation. DFT and ab initio calculations used Gaussian 16.^[52] The analysis of non-covalent interactions in the molecule used the reduced electronic density gradient of Johnson-Contreras.^[39]

Acknowledgements

Funding support from the Spanish Ministerio de Ciencia e Innovación and the European Regional Development Fund (MICINN – ERDF, Grant No. PID2021-125015NB-I00) and the Junta de Castilla y León (Grant Nos. INFRARED IR2020-1-UVa02 and INFRARED IR2021-UVa13) is gratefully acknowledged. W. L. thanks the Chinese Scholarship Council for a research grant. M. J. thanks the Universidad de Valladolid for a “Margarita Salas” postdoctoral contract (CONREC-2021-265).

Conflict of Interests

The authors declare no conflict of interest.

Data Availability Statement

The experimental data corresponding to this investigation are included in the Supporting Information.

Keywords: Thiols · 2-phenylethanethiol · sulfur-centered hydrogen bonds · rotational spectroscopy

[1] S. McLean, D. S. Nichols, N. W. Davies, *PLoS One* **2021**, *16*, e0248961.

[2] W. F. Wood, B. G. Sollers, G. A. Dragoo, J. W. Dragoo, *J. Chem. Ecol.* **2002**, *28*, 1865–1870.

- [3] A. Rutz, M. Sorokina, J. Galgonek, D. Mietchen, E. Willighagen, A. Gaudry, J. G. Graham, R. Stephan, R. Page, J. Vondrášek, C. Steinbeck, G. F. Pauli, J.-L. Wolfender, J. Bisson, P.-M. Allard, *eLife* **2022**, *11*, DOI 10.7554/eLife.70780.
- [4] EFSA Panel on Food Contact Materials, Enzymes, Flavourings and Processing Aids, *EFSA J.* **2012**, *10*, 2455.
- [5] T. Kondo, K. Uosaki, *J. Photochem. Photobiol. C* **2007**, *8*, 1–17.
- [6] P. Cyganik, M. Buck, T. Strunskus, A. Shaporenko, G. Witte, M. Zharnikov, C. Wöll, *J. Phys. Chem. C* **2007**, *111*, 16909–16919.
- [7] R. Karaminkov, S. Chervenkov, H. J. Neusser, *J. Phys. Chem. A* **2008**, *112*, 839–848.
- [8] N. Guchhait, T. Ebata, N. Mikami, *J. Am. Chem. Soc.* **1999**, *121*, 5705–5711.
- [9] M. Mons, E. G. Robertson, L. C. Snoek, J. P. Simons, *Chem. Phys. Lett.* **1999**, *310*, 423–432.
- [10] A. Camiruaga, R. T. Saragi, F. Torres-Hernández, M. Juanes, I. Usabiaga, A. Lesarri, J. A. Fernández, *Phys. Chem. Chem. Phys.* **2022**, *24*, 24800–24809.
- [11] N. Mayorcas, I. Malka, I. Bar, *Phys. Chem. Chem. Phys.* **2011**, *13*, 6808.
- [12] P. D. Godfrey, R. N. Jorissen, R. D. Brown, *J. Phys. Chem. A* **1999**, *103*, 7621–7626.
- [13] R. D. Brown, P. D. Godfrey, *J. Phys. Chem. A* **2000**, *104*, 5742–5746.
- [14] H. S. Biswal, S. Bhattacharyya, A. Bhattacharjee, S. Wategaonkar, *Int. Rev. Phys. Chem.* **2015**, *34*, 99–160.
- [15] A. Chand, D. K. Sahoo, A. Rana, S. Jena, H. S. Biswal, *Acc. Chem. Res.* **2020**, *53*, 1580–1592.
- [16] D. E. Martin, E. G. Robertson, C. D. Thompson, R. J. S. Morrison, *J. Chem. Phys.* **2008**, *128*, 25–27.
- [17] N. W. Larsen, E. Mathier, A. Bauder, H. H. Günthard, *J. Mol. Spectrosc.* **1973**, *47*, 183–188.
- [18] N. W. Larsen, F. M. Nicolaisen, *J. Mol. Struct.* **1974**, *22*, 29–43.
- [19] N. W. Larsen, L. Schulz, *J. Mol. Struct.* **2009**, *920*, 30–39.
- [20] R. T. Saragi, M. Juanes, C. Pérez, P. Pinacho, D. S. Tikhonov, W. Caminati, M. Schnell, A. Lesarri, *J. Phys. Chem. Lett.* **2021**, *12*, 1367–1373.
- [21] R. T. Saragi, M. Juanes, W. Caminati, A. Lesarri, L. Enriquez, M. Jaraiz, *J. Phys. Chem. A* **2019**, *123*, 8435–8440.
- [22] R. T. Saragi, M. Juanes, R. Pinacho, J. E. Rubio, J. A. Fernández, A. Lesarri, *Symmetry* **2021**, *13*, 2022.
- [23] W. Li, R. T. Saragi, M. Juanes, J. Demaison, N. Vogt, A. Fernández-Ramos, A. Lesarri, *J. Chem. Phys.* **2023**, *159*, 1–10.
- [24] W. Caminati, D. Damiani, G. Corbelli, B. Velino, C. W. Bock, *Mol. Phys.* **1991**, *74*, 885–895.
- [25] K. A. Utzat, R. K. Bohn, J. A. Montgomery, H. H. Michels, W. Caminati, *J. Phys. Chem. A* **2010**, *114*, 6913–6916.
- [26] J. K. G. Watson, in *Vib. Spectra Struct. Vol. 6* (Ed.: J. R. Durig), Elsevier B. V., Amsterdam, **1977**, pp. 1–89.
- [27] H. M. Pickett, *J. Mol. Spectrosc.* **1991**, *148*, 371–377.
- [28] P. D. Godfrey, R. D. Brown, *J. Am. Chem. Soc.* **1998**, *120*, 10724–10732.
- [29] G. M. Florio, R. A. Christie, K. D. Jordan, T. S. Zwier, *J. Am. Chem. Soc.* **2002**, *124*, 10236–10247.
- [30] N. A. Seifert, I. A. Finneran, C. Pérez, D. P. Zaleski, J. L. Neill, A. L. Steber, R. D. Suenram, A. Lesarri, S. T. Shipman, B. H. Pate, *J. Mol. Spectrosc.* **2015**, *312*, 13–21.
- [31] F. Xie, N. A. Seifert, M. Heger, J. Thomas, W. Jäger, Y. Xu, *Phys. Chem. Chem. Phys.* **2019**, *21*, 15408–15416.
- [32] H. D. Rudolph, J. Demaison, in *Equilibrium Mol. Struct.* (Eds.: A. Demaison, Jean; Boggs, J.; Csaszar), CRC Press, Boca Raton, FL, **2011**, pp. 125–158.
- [33] K. J. Epple, H. D. Rudolph, *J. Mol. Spectrosc.* **1992**, *152*, 355–376.
- [34] H. D. Rudolph, **2011**. MOMSTRUC Structural computer program package, available from the authors on request
- [35] J. K. G. Watson, A. Roytburg, W. Ulrich, *J. Mol. Spectrosc.* **1999**, *196*, 102–119.
- [36] J. Kraitchman, *Am. J. Phys.* **1953**, *21*, 17–24.
- [37] C. C. Costain, in *Trans. Am. Crystallographic Assoc.* (Eds.: W. F.; Bradley, H. P. Hanson), Polycrystal Book Service, Pittsburgh, **1966**, pp. 157–164.
- [38] J. Demaison, H. D. Rudolph, *J. Mol. Spectrosc.* **2002**, *215*, 78–84.
- [39] J. Contreras-García, E. R. Johnson, S. Keinan, R. Chaudret, J. P. Piquemal, D. N. Beratan, W. Yang, *J. Chem. Theory Comput.* **2011**, *7*, 625–632.
- [40] R. T. Saragi, C. Calabrese, M. Juanes, R. Pinacho, J. E. Rubio, C. Pérez, A. Lesarri, *J. Phys. Chem. Lett.* **2023**, *14*, 207–213.
- [41] Y. Jin, W. Li, R. T. Saragi, M. Juanes, C. Pérez, A. Lesarri, G. Feng, *Phys. Chem. Chem. Phys.* **2023**, *25*, 12174–12181.
- [42] J. L. Neill, S. T. Shipman, L. Alvarez-Valtierra, A. Lesarri, Z. Kisiel, B. H. Pate, *J. Mol. Spectrosc.* **2011**, *269*, 21–29.

- [43] S. T. Shipman, B. H. Pate, in *Handb. High-Resolution Spectrosc.* (Eds.: F. Merkt, M. Quack), John Wiley & Sons, Ltd, New York, **2011**, pp. 801–828.
- [44] J.-U. Grabow, in *Handb. High-Resolution Spectrosc.* (Eds.: F. Merkt, M. Quack), John Wiley & Sons, Ltd, New York, **2011**, pp. 723–799.
- [45] T. A. Halgren, *J. Comput. Chem.* **1999**, *20*, 720–729.
- [46] C. Møller, M. S. Plesset, *Phys. Rev.* **1934**, *46*, 618–622.
- [47] A. D. Becke, *J. Chem. Phys.* **1993**, *98*, 5648–5652.
- [48] S. Grimme, *J. Chem. Phys.* **2006**, *124*, 034108.
- [49] S. Grimme, S. Ehrlich, L. Goerigk, *J. Comput. Chem.* **2011**, *32*, 1456–1465.
- [50] E. R. Johnson, A. D. Becke, *J. Chem. Phys.* **2006**, *124*, 174104.
- [51] F. Weigend, R. Ahlrichs, *Phys. Chem. Chem. Phys.* **2005**, *7*, 3297.
- [52] M. J. Frisch, G. W. Trucks, H. B. Schlegel, G. E. Scuseria, M. A. Robb, J. R. Cheeseman, G. Scalmani, V. Barone, G. A. Petersson, H. Nakatsuji, X. Li, M. Caricato, A. V. Marenich, J. Bloino, B. G. Janesko, R. Gomperts, B. Mennucci, H. P. Hratchian, J. V. Ortiz, A. F. Izmaylov, J. L. Sonnenberg, Williams, F. Ding, F. Lipparini, F. Egidi, J. Goings, B. Peng, A. Petrone, T.

Henderson, D. Ranasinghe, V. G. Zakrzewski, J. Gao, N. Rega, G. Zheng, W. Liang, M. Hada, M. Ehara, K. Toyota, R. Fukuda, J. Hasegawa, M. Ishida, T. Nakajima, Y. Honda, O. Kitao, H. Nakai, T. Vreven, K. Throssell, J. A. Montgomery Jr., J. E. Peralta, F. Ogliaro, M. J. Bearpark, J. J. Heyd, E. N. Brothers, K. N. Kudin, V. N. Staroverov, T. A. Keith, R. Kobayashi, J. Normand, K. Raghavachari, A. P. Rendell, J. C. Burant, S. S. Iyengar, J. Tomasi, M. Cossi, J. M. Millam, M. Klene, C. Adamo, R. Cammi, J. W. Ochterski, R. L. Martin, K. Morokuma, O. Farkas, J. B. Foresman, D. J. Fox, **2016**.

Manuscript received: October 27, 2023

Revised manuscript received: January 19, 2024

Accepted manuscript online: January 28, 2024

Version of record online: February 6, 2024